Journal Pre-proof

Preparation and evaluation of ^{99m}Tc-Labeled HYNIC-Palbociclib analogs for cyclin-dependent kinase 4/6-positive tumor imaging

Qianqian Gan, Xiaoqing Song, Xuran Zhang, Junbo Zhang

PII: S0223-5234(19)31190-0

DOI: https://doi.org/10.1016/j.ejmech.2019.112032

Reference: EJMECH 112032

To appear in: *European Journal of Medicinal Chemistry*

Received Date: 10 November 2019

Revised Date: 24 December 2019

Accepted Date: 31 December 2019

Please cite this article as: Q. Gan, X. Song, X. Zhang, J. Zhang, Preparation and evaluation of ^{99m}Tc-Labeled HYNIC-Palbociclib analogs for cyclin-dependent kinase 4/6-positive tumor imaging, *European Journal of Medicinal Chemistry* (2020), doi: https://doi.org/10.1016/j.ejmech.2019.112032.

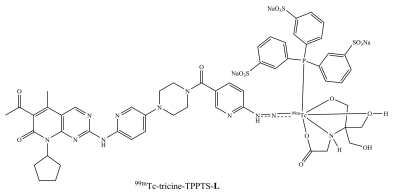

^{99m}Tc-tricine-TPPTS-**L**

Purification free post-labeling

Good water solubility

Specific accumulation in CDK4/6-expressing tumors

Preparation and Evaluation of ^{99m}Tc-Labeled HYNIC-Palbociclib Analogs for Cyclin-Dependent Kinase 4/6-Positive Tumor Imaging

Qianqian Gan[1], Xiaoqing Song[1], Xuran Zhang, Junbo Zhang*

Key Laboratory of Radiopharmaceuticals, Ministry of Education, College of Chemistry, Beijing Normal University, Beijing, 100875, P. R. China.

Abstract

Overexpression and amplification of cyclin-dependent kinase 4/6 (CDK4/6) occur in many cancers and may be the cause of resistance to CDK4/6 inhibitors in preclinical models. However, there are few investigations on the assessment of CDK4/6 expression in tumors or other tissues. Palbociclib, which was approved in 2015 to treat ER+/HER2- breast cancer in combination with letrozole, is a selective CDK4/6 inhibitor. In this study, an intermediate (compound **3**), which could be hydrolyzed into the ligand (compound **L**) consisting of palbociclib as the bioactive molecule and 6-hydrazino nicotinamide (HYNIC) as the bifunctional chelator, was synthesized. Compound **L** was radiolabeled with ^{99m}Tc using tricine/TPPTS or tricine/TPPMS as co-ligands. ^{99m}Tc-tricine-TPPTS-**L** and ^{99m}Tc-tricine-TPPMS-**L** were prepared with high radiochemical purity without postlabeling purification. They had great *in vitro* stability. Both radiotracers were hydrophilic, but ^{99m}Tc-tricine-TPPTS-**L** had a lower log *P* value. *In vitro* cell uptake studies in MCF-7 cells showed that cellular uptake was blocked by preincubation with palbociclib, suggesting a CDK4/6-mediated uptake mechanism. Biodistribution in mice bearing MCF-7 tumors showed that ^{99m}Tc-tricine-TPPTS-**L** had higher tumor uptake than ^{99m}Tc-tricine-TPPMS-**L**, while they had comparable tumor-to-muscle and tumor-to-blood ratios. Radioactivity accumulation in tumors was obvious in micro-SPECT/CT images with ^{99m}Tc-tricine-TPPTS-**L**. When mice were preinjected with palbociclib, tumor uptake of ^{99m}Tc-tricine-TPPTS-**L** significantly decreased and the tumor accumulation was clearly lost, confirming CDK4/6 specificity. All results in this work indicated that ^{99m}Tc-tricine-TPPTS-**L** is a promising tumor imaging agent that targets CDK4/6.

Key words: CDK4/6 · ^{99m}Tc · palbociclib · HYNIC · tumor imaging

1. Introduction

There are four distinct phases (G1, S, G2, M) in the cell cycle. Before entering G1 phase, nondividing cells stay in a resting or quiescence state called G0 phase.[1, 2] Cell cycle dysregulation leads to uncontrolled cell proliferation, subsequently

resulting in tumorigenesis.[3] Specific proteins are in control of the cell cycle. Cyclin-dependent kinases (CDKs), belonging to the serine-threonine protein kinase family, are the primary proteins that regulate the cell cycle. They are triggered by their corresponding cyclins.[4] Among the twenty-one CDKs that have been found already, CDK4 and CDK6 are a pair of CDKs sharing 71% amino acid homology as well as similar functions.[5] They control progression from G1 to S phase through the cyclin D-CDK4/6-INK4-pRb pathway.[6-8] The CDK4/6-cyclin D complex phosphorylates pRb, the product of the antioncogene, causing the dissociation of the pRb-E2F complex. Then, free E2F begins to play the role of a transcription factor to motivate the cell cycle transition from G1 to S phase.[9, 10] Overexpression of CDK4/6 has been observed in many cancers, such as breast cancer[11], oral cancer[12] and glioma[13]. Therefore, selective inhibition of CDK4/6 has been an attractive target for its potential to enhance the chemotherapeutic effects of tumor treatment.[14]

There have also been reports that the amplification of CDK4/6 might be related to the resistance to CDK4/6 inhibitors in preclinical models.[15] Therefore, an assessment of CDK4/6 expression in tumors or other tissues may help to select patients that could be responsive to CDK4/6 inhibitors as well as to reveal the mechanisms of drug resistance. Nuclear medicine technology with the proper tracers can noninvasively achieve this goal at the molecular and cellular levels in living systems. Disappointedly, there have been few investigations on the development of radiotracers targeting CDK4/6 for the diagnosis of cancer. The first reported radiotracers of CDK4 imaging were **[^{124}I]CKIA** and **[^{124}I]CKIB**. Unfortunately, these compounds showed poor performance *in vivo*. They were rapidly metabolized to other substances besides [^{124}I]I_2. Their radioactivity accumulation in FaDu xenografts was unnoteworthy in micro-PET images and only marginal in *ex vivo* autoradiography.[16]

With the development of hardware and image reconstruction methods, the quality of SPECT images has greatly improved. Remarkable physical properties ($t_{1/2}$ = 6 h, E_γ = 140 keV) and convenient availability make ^{99m}Tc still the most widely used radionuclide for SPECT imaging in the clinic. Furthermore, ^{99m}Tc can easily coordinate with biomolecules through a bifunctional chelator, such as isonitrile (-N≡C) and 6-hydrazino nicotinamide (HYNIC). Thus, it has drawn our attention to develop ^{99m}Tc-labeled radiotracers for CDK4/6 imaging.

In our previous work[17], four isocyano-containing palbociclib derivatives were synthesized and radiolabeled with a

[^{99m}Tc(CO)$_3$]$^+$ core. These ^{99m}Tc complexes had good *in vitro* and *in vivo* stability. The corresponding Re chelates showed high affinity for CDK4 and good selectivity for CDK4 versus CDK2 in CDK kinase inhibition assays. A significant reduction of MCF-7 cellular uptake was observed in the presence of palbociclib, indicating a CDK4/6 specific uptake mechanism. Biodistribution studies showed considerable tumor uptake and tumor-to-muscle ratios of all four radiotracers, and the tumor was obviously visible in micro-SPECT/CT images. The results that the tumor uptake of ^{99m}Tc-**L4** could be blocked by excess palbociclib, both in its biodistribution and by micro-SPECT/CT imaging, confirmed its specificity for CDK4/6. However, the highest radioactivity accumulation was found in the abdomen, especially in the liver, which might be due to their good lipophilicity. In this study, we aimed to lower the lipophilicity of ^{99m}Tc-labeled complexes to reduce the uptake in the liver. HYNIC has been a popular and efficient bifunctional chelator for ^{99m}Tc. We maintained the target vector palbociclib but changed the bifunctional chelator to HYNIC. Two ^{99m}Tc-labeled HYNIC-palbociclib complexes using tricine/TPPTS or tricine/TPPMS as co-ligands were prepared and evaluated for their potential to be tumor imaging agents targeting CDK4/6.

2. Results

2.1. Chemistry and radiochemistry

The overall synthesis of compound **3** and the labeling procedures are shown in Scheme 1. A HYNIC-containing active ester (compound **2**) using hydrazone to protect the hydrazine group was synthesized in three steps. Then, palbociclib substituted the NHS ester of **2** under basic conditions to obtain compound **3**, which could be hydrolyzed to produce ligand **L** under acidic conditions (pH 3.5-5.0).[18] All intermediates were characterized by ^{1}H NMR, ^{13}C NMR and MS (spectra are shown in Supplementary data). ^{99m}Tc-tricine-TPPTS-**L** and ^{99m}Tc-tricine-TPPMS-**L** were prepared in one pot. The speculative structures of the complexes are shown in Scheme 1. As shown in Figure 2, the retention time of the ^{99m}Tc chelates were completely different from that of $^{99m}TcO_4^-$ (14.00 min for ^{99m}Tc-tricine-TPPTS-**L**, 16.29 min for ^{99m}Tc-tricine-TPPMS-**L** and 2.67 min for $^{99m}TcO_4^-$). The radiochemical purity of both complexes was over 90%, so purification was not performed in subsequent *in vitro* and *in vivo* studies considering the low concentration of compound **3** used during radiolabeling.

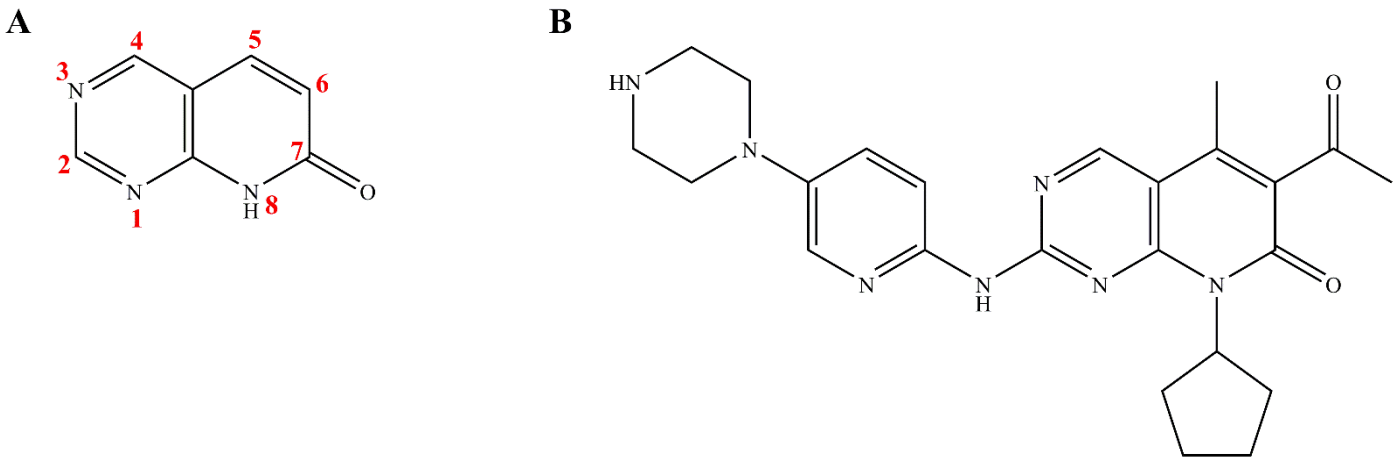

Figure 1. (A) Numbering of the pyrido-[2,3-*d*]pyrimidin-7-one scaffold and (B) the structure of palbociclib.

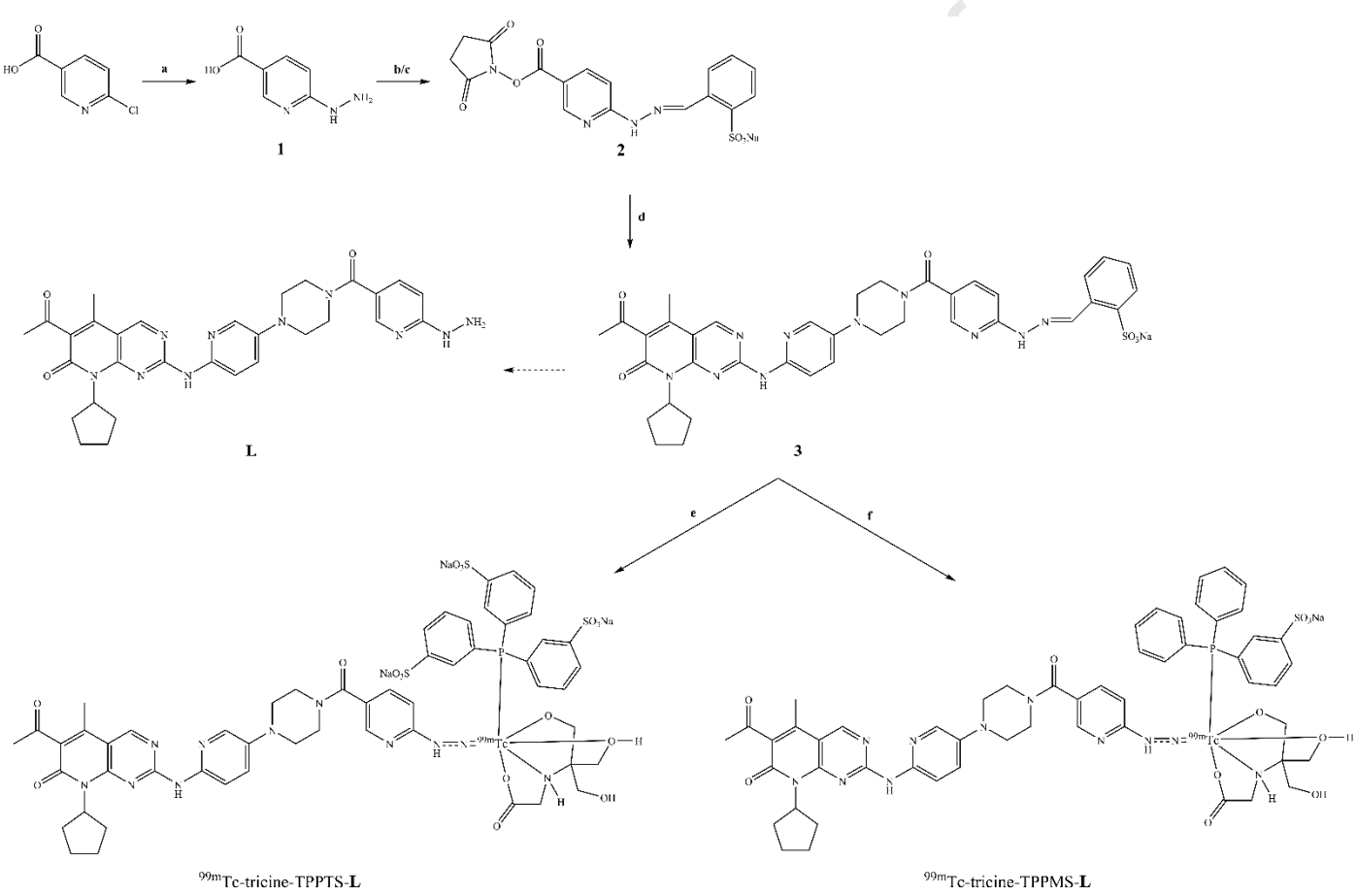

Scheme 1. Synthetic route and speculative structures of ^{99m}Tc-tricine-TPPTS-**L** and ^{99m}Tc-tricine-TPPMS-**L**. Reagents and conditions: **a**. hydrazine hydrate, 100 °C, 4 h; **b**. sodium 2-formylbenzenesulfonate, r.t., 3 h; **c**. *N*-hydroxysuccinimide, DCC, r.t., 18 h→reflux, 1 h; **d**. palbociclib, TEA, DCM, r.t., 6 h; **e**. tricine, TPPTS, $SnCl_2 \cdot 2H_2O$, pH 4-5, $Na^{99m}TcO_4$, 100 °C, 30 min; **f**. tricine, TPPMS, $SnCl_2 \cdot 2H_2O$, pH 4-5, $Na^{99m}TcO_4$, 100 °C, 30 min.

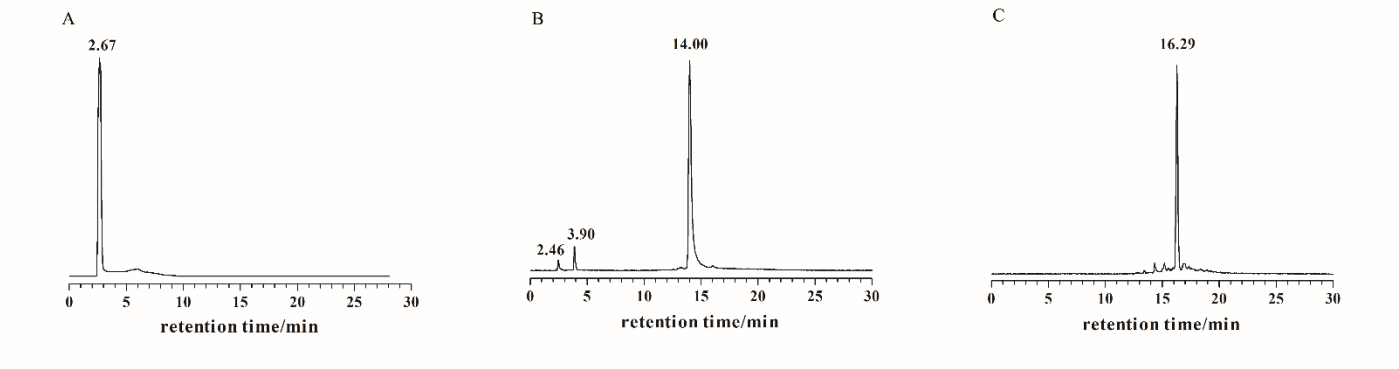

Figure 2. Radiochromatograms of (A) $^{99m}TcO_4^-$, (B) ^{99m}Tc-tricine-TPPTS-**L**, and (C) ^{99m}Tc-tricine-TPPMS-**L**.

2.2. Stability assessment and partition coefficient

The results of the *in vitro* stability assessment (Figure 3) showed that the radiochemical purities of the ^{99m}Tc-labeled radiotracers were still beyond 90% after incubation for 4 h either in the reaction mixture at room temperature or in mouse serum at 37 °C, indicating good *in vitro* stability of both complexes. The log *P* values of ^{99m}Tc-tricine-TPPTS-**L** and ^{99m}Tc-tricine-TPPMS-**L** were -2.951 ± 0.078 and -0.350 ± 0.024, respectively, which demonstrated that they were hydrophilic.

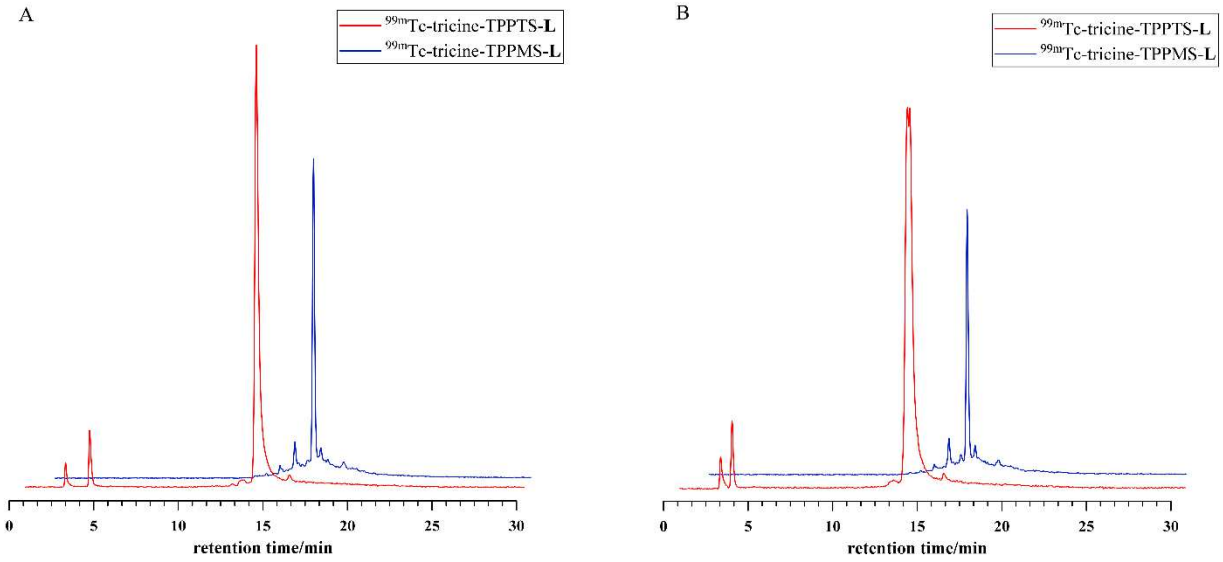

Figure 3. Radiochromatograms of ^{99m}Tc-tricine-TPPTS-**L** (red) and ^{99m}Tc-tricine-TPPMS-**L** (blue) after incubation in the reaction mixture at (A) room temperature or (B) in mouse serum at 37 °C for 4 h.

2.3. Cellular uptake studies

The cellular uptake in the presence of 60 μM of palbociclib decreased by approximately 84% and 27% from unblocked conditions (Figure 4A, $p < 0.05$), respectively. These results indicated a CDK4/6-mediated uptake mechanism. The binding affinity of ^{99m}Tc-tricine-TPPTS-**L** measured by saturation binding assay exhibited a K_d value of 4.68 ± 1.84 nM.

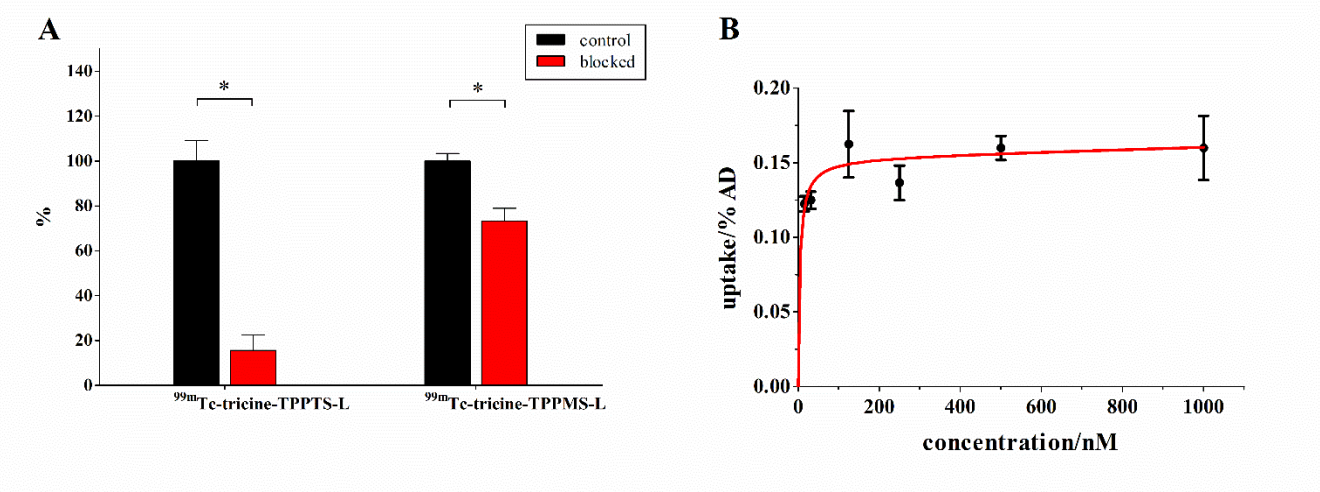

Figure 4. (A) *In vitro* uptake by MCF-7 cells incubated with ^{99m}Tc-labeled tracers in the absence (black column) or presence (red column) of a final concentration of 20 μM palbociclib at 37 °C after 120 min. Statistical analysis was carried out using a bilateral *t* test of equal variance (* $p < 0.05$). (B) Saturation binding study of ^{99m}Tc-tricine-TPPTS-**L** by measuring the cellular uptake at different concentrations as indicated.

2.4. Biodistribution experiments

The biodistribution results of radiotracers ^{99m}Tc-tricine-TPPTS-**L** and ^{99m}Tc-tricine-TPPMS-**L** in MCF-7 xenograft-bearing BALB/c nude mice (n = 3) at 1 and 2 h post-injetion. are shown in Figure 5. MCF-7 tumors showed much higher uptake of ^{99m}Tc-tricine-TPPTS-**L** (3.83 ± 1.33% ID/g at 1 h post-injection and 2.70 ± 0.58% ID/g at 2 h post-injection) than that of ^{99m}Tc-tricine-TPPMS-**L** (0.52 ± 0.04% ID/g at 1 h post-injection and 0.61 ± 0.01% ID/g at 2 h post-injection); the muscle and blood showed similar results, which resulted in comparable ratios of tumor-to-muscle and tumor-to-blood of ^{99m}Tc-tricine-TPPTS-**L** and ^{99m}Tc-tricine-TPPMS-**L**. ^{99m}Tc-tricine-TPPTS-**L** had good retention in the tumor, with approximately 70% radioactivity remaining after 1 h of metabolism. For ^{99m}Tc-tricine-TPPMS-**L**, the tumor uptake even increased slightly at 2 h post-injection compared with that at 1 h post-injection, of which the tracer was also observed in the liver, kidney and spleen. Among the nontargeted tissues, the kidney showed the highest uptake of ^{99m}Tc-tricine-TPPTS-**L**, and the liver had the highest uptake of ^{99m}Tc-tricine-TPPMS-**L**. Low stomach and thyroid (not presented) accumulation implied the absence of $^{99m}TcO_4^-$ *in vivo*. ^{99m}Tc-tricine-TPPTS-**L** had rather high blood uptake at 1 h post-injection but was cleared quickly, with only 57% of the initial uptake being retained at 2 h post-injection. There were few differences in ^{99m}Tc-tricine-TPPMS-**L** uptake in blood between 1 h post-injection and 2 h post-injection.

To assess the specificity for CDK4/6, a group of mice (n = 3) bearing MCF-7 xenografts received palbociclib 30 min prior

to receiving ^{99m}Tc-tricine-TPPTS-**L**. As shown in Figure 5A, the tumor uptake in the blocked mice showed a significant decrease compared with that in the unblocked mice (1.49 ± 0.30% ID/g vs 2.70 ± 0.58% ID/g, p = 0.03), confirming the CDK4/6-mediated tumor uptake mechanism observed *in vitro*.

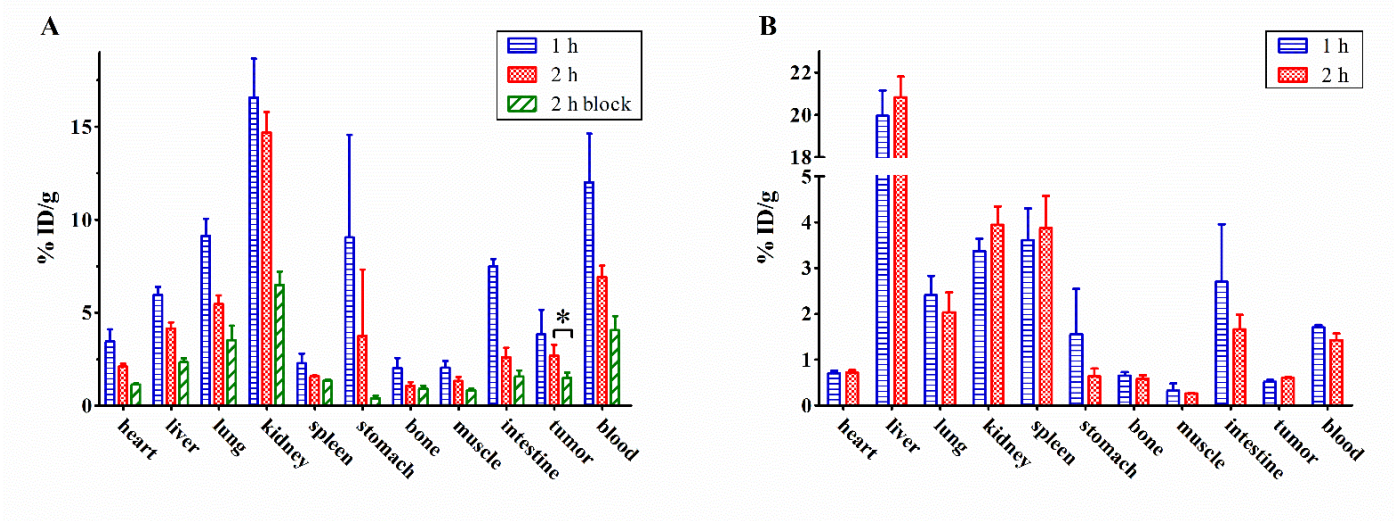

Figure 5. Biodistribution in MCF-7 xenograft-bearing BALB/c nude mice (n = 3) at 1 and 2 h post-injection. (A) ^{99m}Tc-tricine-TPPTS-**L** (* p < 0.05) and (B) ^{99m}Tc-tricine-TPPMS-**L**.

Table 1. Comparison of ^{99m}Tc-labeled tracers in BALB/c nude mice bearing MCF-7 xenografts at 2 h post-injection (mean ± SD[a], % ID/g, n = 3)

	^{99m}Tc-tricine-TPPTS-**L**	^{99m}Tc-tricine-TPPMS-**L**	^{99m}Tc-**L4**
log *P*	-2.951 ± 0.078	-0.350 ± 0.024	1.616 ± 0.066
liver	4.16 ± 0.33	20.84 ± 0.98	62.10 ± 6.71
kidney	14.71 ± 1.09	3.94 ± 0.40	10.97 ± 1.48
spleen	1.59 ± 0.04	3.87 ± 0.70	9.88 ± 1.39
intestine	2.61 ± 0.51	1.66 ± 0.32	0.38 ± 0.10
muscle	1.34 ± 0.21	0.27 ± 0.01	1.92 ± 0.76
tumor	2.70 ± 0.58	0.61 ± 0.01	1.43 ± 0.10
blood	6.92 ± 0.61	1.43 ± 0.14	5.52 ± 0.92

[a] SD is the standard deviation.

2.5. Micro-SPECT/CT imaging

According to the biodistribution results, the tumor uptake of ^{99m}Tc-tricine-TPPMS-**L** was indeed much lower than that of ^{99m}Tc-tricine-TPPTS-**L**. Therefore, a micro-SPECT/CT imaging study was performed with ^{99m}Tc-tricine-TPPTS-**L** in tumor-bearing mice. Because the tumor-to-muscle and tumor-to-blood ratios were enhanced and the uptake decreased over time in the nontarget tissues and organs, such as the kidney and intestine, scans were carried out at 2 h after ^{99m}Tc-tricine-TPPTS-**L** injection. The SPECT/CT images were consistent with the biodistribution results. As seen in Figure

6A, the radioactivity accumulated clearly in the tumor (ROI of 3.94 ± 0.28). The specificity for CDK4/6 was again confirmed by the receptor inhibition study, where the pretreatment of palbociclib suppressed the tumor uptake to a ROI of 0.95 ± 0.18 (Figure 6B).

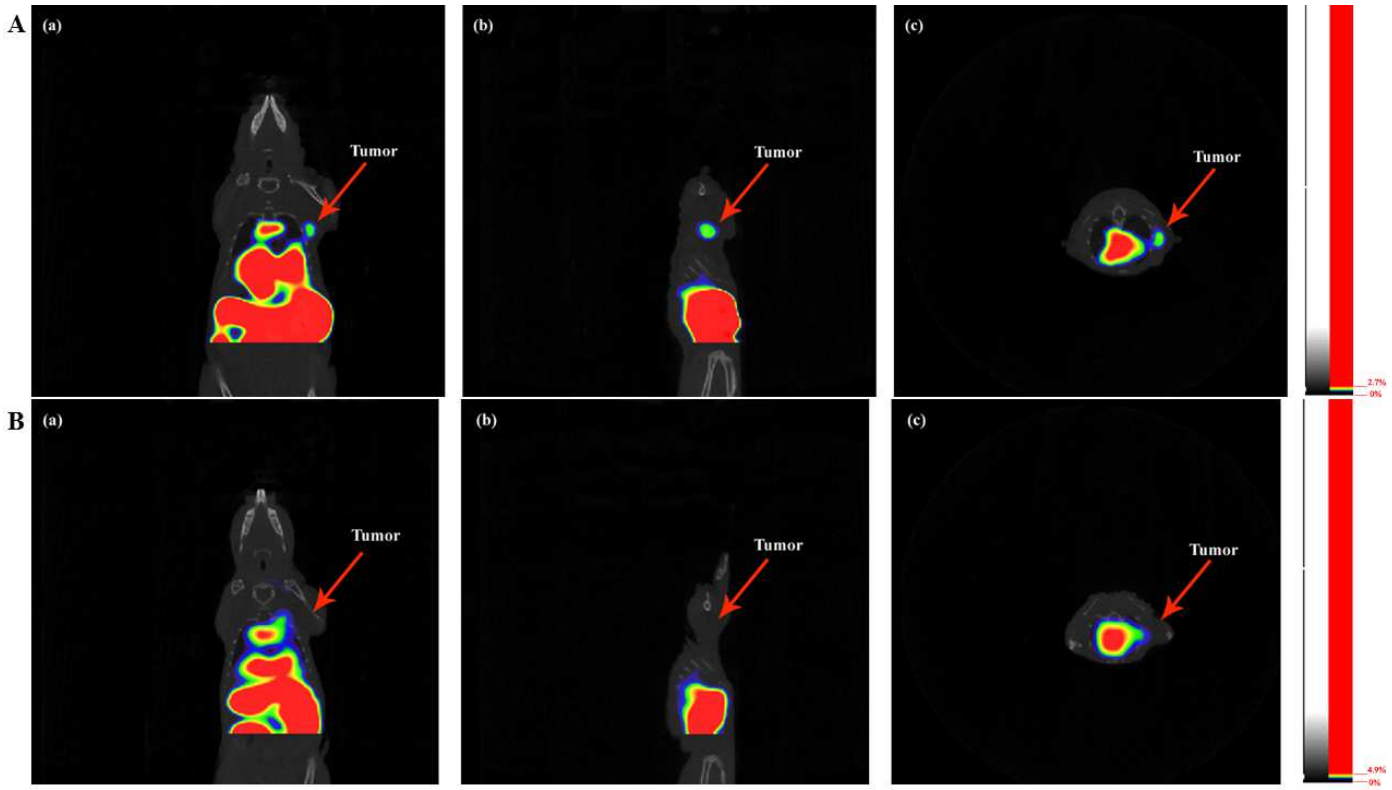

Figure 6. Micro-SPECT/CT images of ^{99m}Tc-tricine-TPPTS-**L** in MCF-7 xenograft-bearing BALB/c nude mice 2 h after radiotracer administration. (A) An unblocked mouse and (B) a blocked mouse. In the blocking study, one hundred micrograms of palbociclib was injected intravenously via the tail vein 30 min before the administration of ^{99m}Tc-tricine-TPPTS-**L**. The images are shown as coronal plane (a), sagittal plane (b) and transverse plane (c).

2.6. Toxicity study

We conducted the MTT assay to determine the cytotoxicity of compound **3**, the prodrug of ligand **L**, in MCF-7 cells. As shown in Figure 7, no remarkable cell death was detected after incubation with compound **3**. In a further abnormal toxicity study, none of five mice showed abnormality or died after 48 h. If one takes a person weighing 60 kg, the dose received by a mouse was 250-278 times as much as a human received per kilogram, suggesting the high safety of the solution of ^{99m}Tc-tricine-TPPTS-**L**.

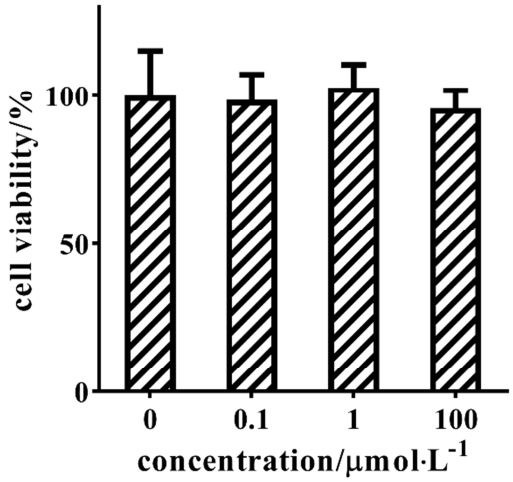

Figure 7. Cell viability after incubation with compound **3** at different concentrations. Each sample was tested in sextuplicate with results given as the mean ± SD.

3. Discussion

Palbociclib, the first selective CDK4/6 inhibitor approved by FDA in 2015, has the potential to be a good and available molecular skeleton to obtain novel ligands for CDK4/6 imaging if the modifications had little interference with the affinity and selectivity. Palbociclib was selected from a subset of pyrido-[2,3-*d*]pyrimidin-7-one scaffolds (Figure 1A) that had favorable selectivity for CDK4.[19] The introduction of the C5 methyl group led to improved selectivity for CDK4.[20] The C6 position appeared to tolerate a range of substituents, but small substituents were preferred. In particular, an acetyl or ethyl ester substituent at the C6 position cooperated better with the C5 methyl group to give rise to an enhancement in potency for CDK4. A cycloalkyl group was required at the N8 position, and a cyclopentyl group held the best balance of potency and selectivity for CDK4.[21] Both the substituents at the C6 and N8 positions occupied the hydrophobic back pocket of the ATP binding pocket.[22, 23] Although substitution of the aniline with a 2-aminopyridine diminished the potency, excellent selectivity for CDK4 was achieved.[21] Studies have revealed that the NH at the C2 position and the nitrogen at the N3 position play a key role in the interaction with the kinase hinge region.[24] The 2-aminopyridine nitrogen is fundamental for CDK4 selectivity. The piperazine moiety attached to the 2-aminopyridine is preferred for its better solubility, but substitution of the piperazine for other heterocyclic groups or modification at the terminal NH position have proven sufferable in light of their small influences on the potency and selectivity.[21, 25] Based on these findings, four ^{99m}Tc-labeling

complexes were prepared successfully and proven to target CDK4/6, which indicated that this combination with a bifunctional chelator for radiometal labeling at NH-piperazine was also practicable. However, their good lipophilicity might be the cause of high liver uptake, which sequentially led to poor quality images.[17] Therefore, it is worth an attempt to lower the lipophilicity by changing the chelator from isocyano-group to others that can chelate with ^{99m}Tc and other hydrophilic co-ligands in further studies. In addition, the bifunctional chelator is expected to form a stable ^{99m}Tc complex with high efficiency at very low amounts of the ligand. The HYNIC moiety is one such chelator that satisfies the above demands. However, it has been reported that the isolated hydrazine group of the HYNIC-biomolecule conjugate was unstable, especially under basic conditions.[18, 26, 27] Aldehydes or ketones extracted from various plastic and rubber materials during preparation could react readily with the hydrazine group to form a hydrazone, which brought about difficulties in maintaining the purity of the ligand. On the other hand, this characteristic could be used to protect the hydrazine group if there was already a hydrazone moiety that was inert to reaction with aldehyde and ketone impurities, formaldehyde in particular, but was not stable enough to hydrolyze under a certain condition to obtain a free hydrazine during radiolabeling. A hydrazone with a 2-sulfonatobenzaldehyde group has been reported to be a good choice.[18, 27] It is inert toward formaldehyde and unstable at pH 3.5-5.0 to form enough of the free hydrazine group during ^{99m}Tc labeling.[18] Furthermore, it is easy to prepare and soluble in water. Compound **2** was synthesized according to the literature,[18] of which the NHS ester could be replaced readily by palbociclib under basic conditions. However, the low solubility of palbociclib in DCM limited the yield of compound **3**.

The preparation of ^{99m}Tc-HYNIC complexes was easy to operate. Not only was labeling accomplished in one pot, but it was also purification free postlabeling since the radiochemical purity was greater than 90% and only 10 μg of compound **3**, the potential bioactive molecule for CDK4/6, had been added. Based on this, for the convenience of ^{99m}Tc labeling, a kit formulation is under consideration.

Choosing HYNIC as the bifunctional chelator has another advantage. Although the certain configuration of ^{99m}Tc-HYNIC complexes has not been confirmed, it is clear that HYNIC occupies only part of the radiolabeling spheres of ^{99m}Tc.[28-32] Therefore, co-ligands are required to complete the unoccupied sites of the ^{99m}Tc coordination spheres, which provides an

opportunity to adjust the efficiency of the labeling yield, the stability of the ^{99m}Tc chelates, and the *in vivo* performance of ^{99m}Tc complexes upon the selection of co-ligands.[31, 33] Tricine is a weakly chelating primary co-ligand, but useful for ligand exchange to obtain more stable and more homogeneous ^{99m}Tc-HYNIC conjugates.[34] TPPTS and TPPMS were used as the secondary co-ligands in this work. As shown in Figure 1, only one new species that definitely had a different retention time from $^{99m}TcO_4^-$ was detected in each labeling mixture by the reversed-phase HPLC method. The speculative structures of ^{99m}Tc-tricine-TPPTS-**L** and ^{99m}Tc-tricine-TPPMS-**L** are depicted in Scheme 1. Two more sulfonic groups make TPPTS more water-soluble than TPPMS. Therefore, it is reasonable that substitution of the co-ligand TPPTS in the complex ^{99m}Tc-tricine-TPPTS-**L** and the co-ligand TPPMS in the complex ^{99m}Tc-tricine-TPPMS-**L** led to a significant decrease in hydrophilicity. Additionally, the trend in the log *P* values was also consistent with the radio-HPLC retention time of each complex, where the retention time of ^{99m}Tc-tricine-TPPTS-**L** was shorter than that of ^{99m}Tc-tricine-TPPMS-**L** (Figure 2). As expected, changing the bifunctional chelator from an alkyl isocyanide to the hydrazinonicotinamide significantly decreased the lipophilicity of the ^{99m}Tc-labeling palbociclib derivatives due to the introduction of water soluble co-ligands, which might reduce the nonspecific uptake in normal organs or tissues such as the liver and small intestine.

The good *in vitro* stability of ^{99m}Tc-tricine-TPPTS-**L** and ^{99m}Tc-tricine-TPPMS-**L** established the foundation for further studies. An internalization study suggested that about 80% of total uptake was found inside the cells at 120 min, consistent with the previous observation that CDK 4/6 were mostly located intracellularly.[35] A significant reduction of uptake in MCF-7 cells was observed with excess treatment with palbociclib, implying a CDK4/6-targeting uptake mechanism. The results of further *in vivo* studies, both biodistribution and micro-SPECT/CT imaging, confirmed this conjecture by blocking experiments. When mice received palbociclib prior to the injection of ^{99m}Tc-tricine-TPPTS-**L**, the tumor uptake and the ROI value decreased by approximately 45% (from 2.70 ± 0.58% ID/g to 1.49 ± 0.30% ID/g) and 76% (from 3.94 ± 0.28 to 0.95 ± 0.18), respectively.

Consistent with previous results, the higher the lipophilicity of the complex, the higher the uptake of the liver.[17, 36] The liver uptake of ^{99m}Tc-tricine-TPPTS-**L** was obviously lower than that of ^{99m}Tc-tricine-TPPMS-**L**, while both were significantly lower than that of the ^{99m}Tc-labeled isocyano-containing palbociclib derivatives (Table 1). The uptake of

^{99m}Tc-tricine-TPPTS-**L** in the kidney was significantly higher than that of ^{99m}Tc-tricine-TPPMS-**L**. This might suggest their different metabolism *in vivo*; renal clearance for the former and a hepatobiliary pathway for the latter. Comparing ^{99m}Tc-tricine-TPPTS-**L** with the most promising CDK4/6 imaging agent ^{99m}Tc-**L4** among ^{99m}Tc-**Ln** (n = 2, 3, 4, 5), although the soluble co-ligands tricine and TPPTS occupied several vector molecules, the tumor uptake showed hardly any interference, while better water solubility (lower log *P* value), lower hepatic and splenic uptake were observed, as shown in Table 1. However, ^{99m}Tc-tricine-TPPTS-**L** failed to reduce blood uptake.

4. Conclusion

In this study, a hydrazone-protected HYNIC-containing NHS ester reacted with palbociclib at the NH-piperazine to successfully obtain compound **3**. The hydrolysate of compound **3**, **L**, was labeled with ^{99m}Tc in the presence of tricine/TPPTS and tricine/TPPMS in high radiochemical yield and radiochemical purity. Both complexes, ^{99m}Tc-tricine-TPPTS-**L** and ^{99m}Tc-tricine-TPPMS-**L**, were hydrophilic and stable for up to 4 h *in vitro*. Palbociclib could significantly suppress the uptake of these complexes in MCF-7 cells as well as the tumor uptake of ^{99m}Tc-tricine-TPPTS-**L** in an MCF-7 tumor-bearing mouse model, which indicated a CDK4/6 specific uptake mechanism. In mice bearing MCF-7 tumors, ^{99m}Tc-tricine-TPPTS-**L** had much higher tumor uptake than ^{99m}Tc-tricine-TPPMS-**L**. In the micro-SPECT/CT imaging study, ^{99m}Tc-tricine-TPPTS-**L** successfully visualized the tumor. Based on the current results, we recommend ^{99m}Tc-tricine-TPPTS-**L** as the best choice of tumor imaging agent with CDK4/6 specificity among ^{99m}Tc-labeled derivatives due to its purification-free preparation, good water solubility and favorable biological performance.

5. Experiments

5.1. Materials

All chemicals were purchased from commercial sources and used without further purification. Palbociclib was obtained from Beijing Lunarsun Pharmaceutical Co. Ltd. *N*-[Tris(hydroxymethyl)methyl]glycine (tricine) was purchased from Ark Pharm. Triphenylphosphine-3,3',3"-trisulfonic acid trisodium salt (TPPTS) and sodium diphenylphosphinobenzene-3-sulfonate (TPPMS) were purchased from TCI (Shanghai) Development Co., Ltd. NMR spectra were obtained on a 400 MHz NMR spectrometer (JOEL). Mass spectra (MS) were recorded on an AB SCIEX

TripleTOF^{TM} 5600 spectrometer (AB Sciex, Concord, Canada). Fresh Na^{99m}TcO$_4$ eluent was obtained from a ^{99}Mo/^{99m}Tc-generator (Chinese Institute of Atomic Energy). Radiochemical purity was analyzed by analytical high-performance liquid chromatography (HPLC) on a Waters 600 binary HPLC pump equipped with a Raytest Gabi radioactivity detector and a Waters 2487 UV absorbance dual λ detector (Milford, MA, USA). A C18 column (5 μm, 250 × 4.6 mm, Kromasil) was used with a flow rate of 1 mL/min in the following system: solvent A, H_2O with 0.1% TFA; and solvent B, CH_3CN with 0.1% TFA (gradient: 0-2 min 10% B, 2-20 min 10-90% B, 20-28 min 90% B, 28-40 min 90-10% B). Radioactivity counts were recorded by a PerkinElmer system (WIZARD^2, 2480 Automatic Gamma Counter). Imaging studies were performed on a Triumph SPECT/CT scanner (TriFoil Imaging, California, USA).

5.2. Chemical synthesis

Compounds **1**-**2** were synthesized according to the reported literature,[27] and the details are shown in the Supplementary data. The synthesis of compound **3** was as follows: Palbociclib (447 mg, 1 mmol) and compound **2** (440 mg, 1 mmol) were added to 30 mL of dichloromethane in a 100 mL round-bottom flask, followed by the addition of 200 μL of trimethylamine. The mixture was allowed to stir at room temperature for 6 h. The solvent was then removed under reduced pressure, and the residue was purified via silica gel column chromatography (dichloromethane/methanol = 10/1) to obtain compound **3** as yellow powder (178 mg, yield 23%). ^{1}H NMR (400 MHz, DMSO-d_6) δ 11.26 (s, 1H), 10.12 (s, 1H), 8.98 (s, 1H), 8.91 (s, 1H), 8.22 (dd, *J* = 2.3, 0.8 Hz, 1H), 8.05 (d, *J* = 2.9 Hz, 1H), 7.99 (dd, *J* = 7.8, 1.4 Hz, 1H), 7.86 (d, *J* = 9.0 Hz, 1H), 7.75 (dd, *J* = 7.7, 1.5 Hz, 1H), 7.70 (dd, *J* = 8.6, 2.3 Hz, 1H), 7.47 (dd, *J* = 9.1, 3.0 Hz, 1H), 7.35-7.30 (m, 1H), 7.28-7.21 (m, 2H), 5.78 (p, *J* = 8.9 Hz, 1H), 3.66 (m, 4H), 3.19 (m, 4H), 2.38 (s, 3H), 2.26 (s, 3H), 2.24-2.15 (m, 2H), 1.90-1.79 (m, 2H), 1.74 (m, 2H), 1.61-1.49 (m, 2H). ^{13}C NMR (100 MHz, DMSO-d_6) δ 203.04, 168.25, 161.28, 159.00, 158.78, 158.39, 155.28, 148.19, 146.36, 145.34, 143.69, 142.62, 141.36, 138.12, 136.53, 132.56, 129.83, 129.27, 128.13, 127.31, 125.96, 125.66, 122.17, 115.51, 107.16, 106.17, 53.49, 49.25, 49.13, 31.83, 28.10, 25.67, 14.16. HRMS (*m/z*): 749.2618 (calc. 749.2618 for $C_{37}H_{37}N_{10}O_6S$ [M-Na]$^-$).

5.3. Radiosyntheses

The radiosynthesis of ^{99m}Tc-tricine-TPPTS-**L** was as follows: In a clean penicillin bottle, tricine (20 mg) and TPPTS (5 mg)

were dissolved in 0.2 mL of saline. After the addition of 25 μL of $SnCl_2 \cdot 2H_2O$ (1 mg/mL in 0.1 N HCl), the pH was adjusted to 4-5. Then, 10 μL of **3** (1 mg/mL in DMF) and 0.5 mL of freshly eluted $Na^{99m}TcO_4$ (37-370 MBq) solution were added. The reaction mixture was incubated at 100 °C for 30 min under vacuum. After cooling to room temperature, the radiochemical yield and purity were analyzed by radio-HPLC. The only difference between the radiosynthesis of ^{99m}Tc-tricine-TPPTS-**L** and ^{99m}Tc-tricine-TPPMS-**L** was the replacement of TPPTS by TPPMS.

5.4. Stability studies

The *in vitro* stability study of ^{99m}Tc-labeled **L** was in accordance with the literature.[37] In brief, 200 μL of the reaction mixture was kept at room temperature or incubated in 200 μL of mouse serum at 37 °C. After 4 h, an aliquot of the reaction mixture was loaded onto the HPLC for assessment of the radiochemical purity.

5.5. Determination of the partition coefficient

To evaluate the hydrophilicity of ^{99m}Tc-labeled complexes, the partition coefficient between 1-octanol and phosphate buffer (0.025 mol/L, pH 7.4) was determined according to the method described previously.[37] The final partition coefficient value was expressed as log $P \pm$ SD.

5.6. Cell culture and tumor models

The human breast adenocarcinoma MCF-7 cell line was purchased from the Chinese Infrastructure of Cell Line Resource and cultured in DMEM containing 10% FBS (fetal bovine serum) and 1% penicillin-streptomycin in a humidified incubator at 37 °C with 5% CO_2. Female BALB/c nude mice (18-20 g) were obtained from Beijing Vital River Laboratory Animal Technology Co., Ltd. The left armpit of the mice were inoculated subcutaneously with nearly 1×10^7 cells in 0.1 mL of DMEM. After 7-10 days, biodistribution and micro-SPECT/CT imaging studies were carried out when the tumors reached 5-10 mm in diameter.

5.7. Cell studies

To demonstrate whether the uptake of the complexes by the tumor cells was CDK4/6-mediated, MCF-7 cells (2×10^5 cells/well in 24-well plates) were pretreated with palbociclib (60 μM/well) for 30 min. Then, ^{99m}Tc-tricine-TPPTS-**L** or ^{99m}Tc-tricine-TPPMS-**L** (7.4 kBq) was added followed by incubation at 37 °C for 2 h. The cells were then rinsed with 0.5

mL of cold PBS with 0.2% BSA twice and lysed with 0.5 mL of 1 M NaOH. Radioactivity counts were measured with a γ-counter. The experiment was repeated in triplicate.

Saturation binding assays were performed as described in the literature.[38] In brief, approximately 2 × 10^4 MCF-7 cells were seeded in every well of 96-well plates and allowed to attach overnight. After removal of the medium, ^{99m}Tc-tricine-TPPTS-**L** at different concentrations (15-1000 nM) was added followed by incubation with the cells at 37 ℃ for 1 h. Post-incubation treatments were the same as described above. The radioactivity was expressed as the percentage of applied activity. The resulting data was used for determining the potency of ^{99m}Tc-tricine-TPPTS-**L** against CDK4/6 by calculating the dissociation constant (K_d), which was calculated by GraphPad Prism 5.0. Each assay was performed four times in parallel.

5.8. Biodistribution experiments

For biodistribution studies, every MCF-7 tumor-bearing mouse received 0.1 mL of ^{99m}Tc-tricine-TPPTS-**L** or ^{99m}Tc-tricine-TPPMS-**L** (74 kBq) by intravenous injection via the tail vein. Mice were sacrificed by decapitation at 1 or 2 h post-injection. The tumor, blood and other tissues of interest (liver, lung, kidney, spleen, stomach, small intestine, bone, muscle and thyroid) were harvested, weighed and measured for their radioactivity via a γ-counter. The radioactivity of every organ or tissue was expressed as the percent uptake of the injected dose per gram of tissue (% ID/g). To confirm the CDK4/6-specific uptake by tumors, we performed a blocking study. In the blocking group, mice were injected with 100 μg of palbociclib 30 min before the injection of ^{99m}Tc-tricine-TPPTS-**L** (74 kBq). Mice were sacrificed at 2 h post-injection.

5.9. Micro-SPECT/CT imaging

MCF-7 tumor-bearing BALB/c nude mice (n = 3) were injected intravenously with 0.1-0.2 mL of ^{99m}Tc-tricine-TPPTS-**L** (18.5 MBq). Acquisition of SPECT/CT images was performed while the mice were anesthetized with 1.5% isoflurane in air at 500 mL/min at 120 min post-injection. A blocking study was also carried out in the micro-SPECT/CT imaging study. On the same day, another mouse was pretreated with 100 μg of palbociclib by i.v. injection via the tail vein, followed by 0.1-0.2 mL of ^{99m}Tc-tricine-TPPTS-**L** (18.5 MBq). Then, a SPECT/CT scan was acquired 2 h later by means of the same method. A protocol consisting of an SPECT acquisition (peak 140 keV, 20% width, no rotation, MMP930 collimator) for 20 min and a

CT scan (512 views, 2 × 2 binding, 75 kV, exposure time 230 ms) for 4 min was performed. The SPECT/CT images were acquired using the HiSPECT software and the VivoQuant 2.5 software.

5.10.Toxicity study

To evaluate the cytotoxicity of compound **3**, MTT assay were carried out in MCF-7 cells according to the literature.[39] Briefly, MCF-7 cells were seeded in a 96-well plate (5000 cells/well) and incubated for attachment. After a night, different concentrations (0.1, 1, 100 μM) of compound **3** were added and incubated with cells for 24 h. Then, after the addition of MTT solution (5 mg/mL), cells were incubated at 37 °C in darkness for another 4 h. At the end of incubation, the culture media were removed after centrifugation. 50 μL of DMSO was added to each well to dissolve the purple crystal. The absorbance of each well at 570 nm was measured using 1420 Multiabel counter. For most radiopharmaceuticals, the abnormal toxicity was within consideration. Therefore, we studied the toxicity of the solution of ^{99m}Tc-tricine-TPPTS-**L** according to the regulation of pharmacopoeia of People's Republic of China (2015 Edition). The total volume of the reaction mixture was adjusted to 6 mL with saline after radiolabeling. Then, 0.5 mL of this solution were injected to Kunming mice (n = 5, female, 18-20 g) via the tail vein. The toxicity of the solution was determined by observing the death and survival of mice in the next 48 h.

Compliance with ethical standards

All animal studies were performed according to the Regulations on Laboratory Animals of Beijing Municipality.

Author Information

Corresponding Author

*zhjunbo@bnu.edu.cn

ORCID: Junbo Zhang: 0000-0003-3549-6483

Present Addresses

No. 19 Xinjiekou Wai Boulevard, Haidian District, Beijing. College of Chemistry, Beijing Normal University, 100875, P. R. (China).

Author Contributions

[1] Qianqian Gan and Xiaoqing Song contributed equally to this work.

Notes

The authors confirm that this article content has no conflicts of interest.

Acknowledgments

The work was financially supported by the National Natural Science Foundation of China (21771023) and the project of the Beijing Municipal Science and Technology Commission (Z181100002218033).

Appendix A. Supplementary data

Synthesis of compound **1-2**, ^{1}H-NMR, ^{13}C-NMR, and MS spectra are listed in the supporting information.

References

[1] K. Vermeulen, D.R. Van Bockstaele, Z.N. Berneman, The Cell Cycle: A Review of Regulation, Deregulation and Therapeutic Targets in Cancer, Cell Proliferat. 36 (2003) 131-149. http://doi.org/10.1046/j.1365-2184.2003.00266.x

[2] H.P. Wagner, Cell Cycle Control and Cancer, Indian J. Pediatr. 65 (1998) 805-814. http://doi.org/10.1007/BF02831338

[3] L.H. Hartwell, M.B. Kastan, Cell-Cycle Control and Cancer, Science 266 (1994) 1821-1828. http://doi.org/10.1126/science.7997877

[4] S.R. Whittaker, A. Mallinger, P. Workman, P.A. Clarke, Inhibitors of Cyclin-Dependent Kinases as Cancer Therapeutics, Pharmacol. Therapeut. 173 (2017) 83-105. http://doi.org/10.1016/j.pharmthera.2017.02.008

[5] M.J. Grossel, P.W. Hinds, From Cell Cycle to Differentiation - an Expanding Role for Cdk6, Cell Cycle 5 (2006) 266-270. http://doi.org/10.4161/cc.5.3.2385

[6] E. Hamilton, J.R. Infante, Targeting CDK4/6 in Patients with Cancer, Cancer Treat. Rev. 45 (2016) 129-138. http://doi.org/10.1016/j.ctrv.2016.03.002

[7] C.J. Sherr, D. Beach, G.I. Shapiro, Targeting CDK4 and CDK6: From Discovery to Therapy, Cancer Discov. 6 (2016) 353-367. http://doi.org/10.1158/2159-8290.CD-15-0894

[8] T. VanArsdale, C. Boshoff, K.T. Arndt, R.T. Abraham, Molecular Pathways: Targeting the Cyclin D-CDK4/6 Axis for Cancer Treatment, Clin. Cancer Res. 21 (2015) 2905-2910. http://doi.org/10.1158/1078-0432.CCR-14-0816

[9] C.J. Sherr, Mammalian G(1)-Cyclins, Cell 73 (1993) 1059-1065. http://doi.org/10.1016/0092-8674(93)90636-5

[10] J.A. Diehl, Cycling to Cancer with Cyclin D1, Cancer Biol. Ther. 1 (2002) 226-231. http://doi.org/10.4161/cbt.72

[11] A.F. de Groot, C.J. Kuijpers, J.R. Kroep, CDK4/6 Inhibition in Early and Metastatic Breast Cancer: A Review, Cancer Treat. Rev. 60 (2017) 130-138. http://doi.org/10.1016/j.ctrv.2017.09.003

[12] S. Poomsawat, W. Buajeeb, S. Khovidhunkit, J. Punyasingh, Alteration in the Expression of Cdk4 and Cdk6 Proteins in Oral Cancer and Premalignant Lesions, J. Oral Pathol. Med. 39 (2010) 793-799. http://doi.org/10.1111/j.1600-0714.2010.00909.x

[13] C.W. Brennan, R.G.W. Verhaak, A. McKenna, B. Campos, H. Noushmehr, S.R. Salama, S. Zheng, D. Chakravarty, J.Z. Sanborn, S.H. Berman, R. Beroukhim, B. Bernard, C. Wu, G. Genovese, I. Shmulevich, J. Barnholtz-Sloan, L. Zou, R. Vegesna, S.A. Shukla, G. Ciriello, W.K. Yung, W. Zhang, C. Sougnez, T. Mikkelsen, K. Aldape, D.D. Bigner, E.G. Van Meir, M. Prados, A. Sloan, K.L. Black, J. Eschbacher, G. Finocchiaro, W. Friedman, D.W. Andrews, A. Guha, M. Iacocca, B.P. O'Neill, G. Foltz, J. Myers, D.J. Weisenberger, R. Penny, R. Kucherlapati, C.M. Perou, D.N. Hayes, R. Gibbs, M. Marra, G.B. Mills, E. Lander, P. Spellman, R. Wilson, C. Sander, J. Weinstein, M. Meyerson, S. Gabriel, P.W. Laird, D. Haussler, G. Getz, L. Chin, T.R. Network, The Somatic Genomic Landscape of Glioblastoma, Cell 155 (2013) 462-477. http://doi.org/10.1016/j.cell.2013.09.034

[14] G.I. Shapiro, Cyclin-Dependent Kinase Pathways as Targets for Cancer Treatment, J. Clin. Oncol. 24 (2006) 1770-1783. http://doi.org/10.1200/JCO.2005.03.7689

[15] K. Pandey, H. An, S.K. Kim, S.A. Lee, S. Kim, S.M. Lim, G.M. Kim, J. Sohn, Y.W. Moon, Molecular Mechanisms of Resistance to CDK4/6 Inhibitors in Breast Cancer: A Review, Int. J. Cancer 145 (2019) 1179-1188. http://doi.org/10.1002/ijc.32020

[16] L. Koehler, F. Graf, R. Bergmann, J. Steinbach, J. Pietzsch, F. Wuest, Radiosynthesis and Radiopharmacological Evaluation of Cyclin-Dependent Kinase 4 (Cdk4) Inhibitors, Eur. J. Med. Chem. 45 (2010) 727-737. http://doi.org/10.1016/j.ejmech.2009.11.020

[17] X. Song, Q. Gan, X. Zhang, J. Zhang, Synthesis and Biological Evaluation of Novel ^{99m}Tc-Labeled Palbociclib Derivatives Targeting Cyclin-Dependent Kinase 4/6 (CDK4/6) as Potential Cancer Imaging Agents, Mol. Pharmaceutics 16 (2019) 4213-4222. http://doi.org/10.1021/acs.molpharmaceut.9b00540

[18] D.S. Edwards, S. Liu, A.R. Harris, M.J. Poirier, B.A. Ewels, Tc-99m-Labeling of Hydrazones of a Hydrazinonicotinamide Conjugated Cyclic Peptide, Bioconjugate Chem. 10 (1999) 803-807. http://doi.org/10.1021/bc990022e

[19] D.W. Fry, P.J. Harvey, P.R. Keller, W.L. Elliott, M.A. Meade, E. Trachet, M. Albassam, X.X. Zheng, W.R. Leopold, N.K. Pryer, P.L. Toogood, Specific Inhibition of Cyclin-Dependent Kinase 4/6 by PD 0332991 and Associated Antitumor Activity in Human Tumor

Xenografts, Mol. Cancer Ther. 3 (2004) 1427-1437.

[20] S.N. VanderWel, P.J. Harvey, D.J. McNamara, J.T. Repine, P.R. Keller, J. Quin, R.J. Booth, W.L. Elliott, E.M. Dobrusin, D.W. Fry, P.L. Toogood, Pyrido[2,3-*d*]Pyrimidin-7-Ones as Specific Inhibitors of Cyclin-Dependent Kinase 4, J. Med. Chem. 48 (2005) 2371-2387. http://doi.org/10.1021/jm049355+

[21] P.L. Toogood, P.J. Harvey, J.T. Repine, D.J. Sheehan, S.N. VanderWel, H.R. Zhou, P.R. Keller, D.J. McNamara, D. Sherry, T. Zhu, J. Brodfuehrer, C. Choi, M.R. Barvian, D.W. Fry, Discovery of a Potent and Selective Inhibitor of Cyclin-Dependent Kinase 4/6, J. Med. Chem. 48 (2005) 2388-2406. http://doi.org/10.1021/jm049354h

[22] M. Barvian, D.H. Boschelli, J. Cossrow, E. Dobrusin, A. Fattaey, A. Fritsch, D. Fry, P. Harvey, P. Keller, M. Garrett, F. La, W. Leopold, D. McNamara, M. Quin, S. Trumpp-Kallmeyer, P. Toogood, Z.P. Wu, E.L. Zhang, Pyrido[2,3-*d*]Pyrimidin-7-One Inhibitors of Cyclin-Dependent Kinases, J. Med. Chem. 43 (2000) 4606-4616. http://doi.org/10.1021/jm000271k

[23] M. Poratti, G. Marzaro, Third-Generation CDK Inhibitors: A Review On the Synthesis and Binding Modes of Palbociclib, Ribociclib and Abemaciclib, Eur. J. Med. Chem. 172 (2019) 143-153. http://doi.org/10.1016/j.ejmech.2019.03.064

[24] B. Nagar, W.G. Bornmann, P. Pellicena, T. Schindler, D.R. Veach, W.T. Miller, B. Clarkson, J. Kuriyan, Crystal Structures of the Kinase Domain of c-Abl in Complex with the Small Molecule Inhibitors PD173955 and Imatinib (STI-571), Cancer Res. 62 (2002) 4236-4243.

[25] P. Wang, J. Huang, K. Wang, Y. Gu, New Palbociclib Analogues Modified at the Terminal Piperazine Ring and their Anticancer Activities, Eur. J. Med. Chem. 122 (2016) 546-556. http://doi.org/https://doi.org/10.1016/j.ejmech.2016.07.020

[26] D.A. Schwartz, M.J. Abrams, C.M. Giadomenico, J.A. Zubieta, Certain Pyridyl Hydrazines and Hydrazides Useful for Protein Labeling. *U.S. Patent 5,206,370*, **1993**.

[27] T.D. Harris, M. Sworin, N. Williams, M. Rajopadhye, P.R. Damphousse, D. Glowacka, M.J. Poirier, K. Yu, Synthesis of Stable Hydrazones of a Hydrazinonicotinyl-Modified Peptide for the Preparation of Tc-99m-labeled Radiopharmaceuticals, Bioconjugate Chem. 10 (1999) 808-814. http://doi.org/10.1021/bc9900237

[28] R.C. King, M.B. Surfraz, S.C.G. Biagini, P.J. Blower, S.J. Mather, How Do HYNIC-Conjugated Peptides Bind Technetium? Insights from LC-MS and Stability Studies, Dalton T. (2007) 4998-5007. http://doi.org/10.1039/b705111e

[29] S. Liu, Bifunctional Coupling Agents for Radiolabeling of Biomolecules and Target-Specific Delivery of Metallic Radionuclides, Adv. Drug Deliver. Rev. 60 (2008) 1347-1370. http://doi.org/10.1016/j.addr.2008.04.006

[30] L.K. Meszaros, A. Dose, S.C.G. Biagini, P.J. Blower, Synthesis and Evaluation of Analogues of HYNIC as Bifunctional Chelators for Technetium, Dalton T. 40 (2011) 6260-6267. http://doi.org/10.1039/c0dt01608j

[31] J.W. Babich, A.J. Fischman, Effect of Co-Ligand on the Biodistribution of Tc-99m-Labeled Hydrazino Nicotinic-Acid Derivatized Chemotactic Peptides, Nucl. Med. Biol. 22 (1995) 25-30. http://doi.org/10.1016/0969-8051(94)00081-T

[32] J.W. Babich, H. Solomon, M.C. Pike, D. Kroon, W. Graham, M.J. Abrams, R.G. Tompkins, R.H. Rubin, A.J. Fischman, Tc-99m-Labeled Hydrazino-Nicotinamide Derivatized Chemotactic Peptide Analogs for Imaging Focal Sites of Bacterial-Infection, J. Nucl. Med. 34 (1993) 1964-1974.

[33] J.W. Babich, W. Graham, S.A. Barrow, A.J. Fischman, Comparison of the Infection Imaging Properties of a Tc-99m Labeled Chemotactic Peptide with In-111 IgG, Nucl. Med. Biol. 22 (1995) 643-648. http://doi.org/10.1016/0969-8051(94)00138-A

[34] C. Decristoforo, B. Faintuch-Linkowski, A. Rey, E. von Guggenberg, M. Rupprich, I. Hernandez-Gonzales, T. Rodrigo, R. Haubner, [99mTc]HYNIC-RGD for Imaging Integrin $\alpha_v\beta_3$ Expression, Nucl. Med. Biol. 33 (2006) 945-952. http://doi.org/10.1016/j.nucmedbio.2006.09.001

[35] Y. Xiong, T. Li, G. Assani, H. Ling, Q. Zhou, Y. Zeng, F. Zhou, Y. Zhou, Ribociclib, a Selective Cyclin D Kinase 4/6 Inhibitor, Inhibits Proliferation and Induces Apoptosis of Human Cervical Cancer in Vitro and in Vivo, Biomed. Pharmacother. 112 (2019) 108602. http://doi.org/10.1016/j.biopha.2019.108602

[36] J.A. Barrett, A.C. Crocker, D.J. Damphousse, S.J. Heminway, S. Liu, D.S. Edwards, J.L. Lazewatsky, M. Kagan, T.J. Mazaika, T.R. Carroll, Biological Evaluation of Thrombus Imaging Agents Utilizing Water Soluble Phosphines and Tricine as Coligands When Used to Label a Hydrazinonicotinamide-Modified Cyclic Glycoprotein IIb/IIIa Receptor Antagonist with Tc-99m, Bioconjugate Chem. 8 (1997) 155-160. http://doi.org/10.1021/bc970001p

[37] T. Liu, Q. Gan, J. Zhang, Z. Jin, W. Zhang, Y. Zhang, Synthesis and Biodistribution of Novel (TcN)-Tc-99m Complexes of Glucose Dithiocarbamate as Potential Probes for Tumor Imaging, Medicinal Chemistry Communications 7 (2016) 1381-1386. http://doi.org/10.1039/c6md00127k

[38] T. Liu, C. Liu, X. Xu, F. Liu, X. Guo, N. Li, X. Wang, J. Yang, X. Yang, H. Zhu, Z. Yang, Preclinical Evaluation and Pilot Clinical Study of (AlF)-F-18-PSMA-BCH for Prostate Cancer PET Imaging, J. Nucl. Med. 60 (2019) 1284-1292. http://doi.org/10.2967/jnumed.118.221671

[39] Y. Li, K. Wang, K. Zhou, W. Guo, B. Dai, Y. Liang, J. Dai, M. Cui, Novel D-A-D Based Near-Infrared Probes for the Detection of Beta-Amyloid and Tau Fibrils in Alzheimer's Disease, Chem. Commun. 54 (2018) 8717-8720. http://doi.org/10.1039/c8cc05259j

Highlights

1. Two ^{99m}Tc-labeled HYNIC-palbociclib analogs were prepared as cyclin-dependent kinase 4/6-positive tumor imaging agents.
2. A CDK4/6-mediated uptake mechanism in MCF-7 cells was observed.
3. ^{99m}Tc-tricine-TPPTS-**L** showed specific accumulation in CDK4/6-expressing tumors at 2 h post-injection.

Declaration of interests

☒ The authors declare that they have no known competing financial interests or personal relationships that could have appeared to influence the work reported in this paper.

☐The authors declare the following financial interests/personal relationships which may be considered as potential competing interests:

The authors declare no conflicts of interest. All authors have given approval to the final version of the manuscript.